Article

SOURCE DATA | TRANSPARENT PROCESS

THE EMBO JOURNAL

Bacteria elicit a phage tolerance response subsequent to infection of their neighbors

Elhanan Tzipilevich[†,‡], Osher Pollak-Fiyaksel[†], Bushra Shraiteh & Sigal Ben-Yehuda*

Abstract

Appearance of plaques on a bacterial lawn is a sign of successive rounds of bacteriophage infection. Yet, mechanisms evolved by bacteria to limit plaque spread have been hardly explored. Here, we investigated the dynamics of plaque development by lytic phages infecting the bacterium *Bacillus subtilis*. We report that plaque expansion is followed by a constriction phase owing to bacterial growth into the plaque zone. This phenomenon exposed an adaptive process, herein termed "phage tolerance response", elicited by non-infected bacteria upon sensing infection of their neighbors. The temporary phage tolerance is executed by the stress-response RNA polymerase sigma factor σ^X (SigX). Artificial expression of SigX prior to phage attack largely eliminates infection. SigX tolerance is primarily conferred by activation of the *dlt* operon, encoding enzymes that catalyze D-alanylation of cell wall teichoic acid polymers, the major attachment sites for phages infecting Gram-positive bacteria. D-alanylation impedes phage binding and hence infection, thus enabling the uninfected bacteria to form a protective shield opposing phage spread.

Keywords *Bacillus subtilis*; bacteriophage; cell wall teichoic acid; *dlt* operon; plaque formation

Subject Categories Microbiology, Virology & Host Pathogen Interaction

DOI 10.15252/embj.2021109247 | Received 21 July 2021 | Revised 8 November 2021 | Accepted 12 November 2021 | Published online 8 December 2021

The EMBO Journal (2022) 41: e109247

See also: **EE Maffei & A Harms** (February 2022)

Introduction

Plaques, reporting bacterial clearance, are the hallmark of bacteriophage (phage) infection since the pioneering discoveries made by Twort and d'Herelle at the beginning of the 20th century (Twort, 1914; d'Hérelles, 1917; Chanishvili, 2012). Plaques are basically visible holes, formed on a lawn of bacteria grown on a solid surface, that report bacterial clearance following successive cycles of infection, including phage adsorption, replication, and spread to nearby hosts. Intriguingly, plaques exhibit a considerable variation in shape according to the host and the infecting phage and are predominantly restricted in size (Abedon & Yin, 2009). It has been proposed that such size limitation is achieved, at least in part, by the entry of bacteria into stationary phase, which frequently restrains phage replication (Abedon & Yin, 2009). However, although plaque employment as a method for monitoring phage infection began decades ago, relatively little is known about the kinetics of plaque development. Furthermore, factors limiting plaque size and expansion are mostly unrevealed.

In this study, we investigated the dynamics of plaque formation, utilizing the Gram-positive soil bacterium *Bacillus subtilis* (*B. subtilis*) and its lytic phages SPP1 and Phi29. Binding of phages to *B. subtilis* is commonly mediated by wall teichoic acid (WTA) polymers, a diverse family of cell surface glycopolymers containing phosphodiester-linked glycerol repeat units poly(Gro-P), decorated by glucose and D-alanine moieties, and anchored to peptidoglycan (PG) through an N-acetylmannosaminyl (Brown *et al*, 2013). WTA polymers were found to be crucial surface components, required for invasion by manifold phages into Gram-positive bacteria such as *Bacilli*, *Listeria,* and *Staphylococci* (Lindberg, 1973; Habusha *et al*, 2019; Ingmer *et al*, 2019; Sumrall *et al*, 2020). SPP1, a double-stranded DNA (dsDNA) phage (44 kb) and a member of the Siphoviridae family, characterized by a long noncontractile tail (Alonso *et al*, 1997), initiates infection by reversible binding of the tail tip to poly-glycosylated WTA (gWTA). Subsequently, SPP1 binds irreversibly to its membrane receptor protein YueB, resulting in DNA injection into the bacterium cytoplasm (Sao-Jose *et al*, 2004; Baptista *et al*, 2008). Phi29 phage, which is significantly smaller (19.3 kb) and belongs to the Podoviridae family, harboring a short noncontractile tail (Salas, 2012), was shown to entirely rely on intact gWTA for infection (Young, 1967). The fact that phages assigned to distinct families utilize gWTA to invade the host strengthens the vital role of these polymers in host recognition by phages and implicates them as major elements for host cell vulnerability. Consistent with this notion, we have shown that a mutant bacteriophage capable of bypassing the need for binding the glucosyl residues, decorating the WTA polymers, gained a broader host range, as it could infect non-host bacterial species presenting dissimilar glycosylation patterns (Habusha *et al*, 2019).

Department of Microbiology and Molecular Genetics, Institute for Medical Research Israel-Canada (IMRIC), The Hebrew University-Hadassah Medical School, The Hebrew University of Jerusalem, Jerusalem, Israel
*Corresponding author. Tel: +972 2 6758600; E-mail: sigalb@ekmd.huji.ac.il
[†]These authors contributed equally to this work
[‡]Present address: Department of Biology and Howard Hughes Medical Institute, Duke University, Durham, North Carolina, USA

Previously, we demonstrated that phages could occasionally invade resistant cells that acquire phage receptors from their sensitive neighbors, highlighting the importance of understanding infection dynamics in a temporal and spatial fashion (Tzipilevich *et al*, 2017). Here, we visualized plaques formed on a lawn of *B. subtilis* bacteria. We revealed that plaque spreading is followed by a phase of constriction mediated by bacterial regrowth into the plaque zone. Characterization of the plaque constriction phase uncovered a temporary immunity mechanism, propelled by a programed transcriptional response, enabling bacteria to tolerate infection by remodeling WTA polymers. This modification reduces phage binding and restricts phage spread. Unlike other mechanisms affording long-term bacterial immunity to phages, namely, restriction enzymes and CRISPR (Labrie *et al*, 2010), this tolerance mechanism confers a transient adaptive response, providing protection to the uninfected bacterial population subsequent to infection of their neighbors.

Results

Plaque expansion is followed by a phase of plaque constriction

To explore the bacterial population dynamic during phage attack on solid surfaces, we followed the process of plaque formation by SPP1 on a lawn of mCherry-labeled *B. subtilis* cells at high resolution, using time-lapse confocal microscopy. Maximal SPP1 plaque size was detected approximately eight hours postinfection, but remarkably the spread was counteracted by bacteria growing into the plaque area, limiting plaque expansion (Fig 1A; Movie EV1). Consequently, the final plaque diameter measured after overnight incubation was significantly smaller than the maximal size reached during plaque development (Fig 1A). To further explore this phenomenon, we followed the kinetics of plaque formation on agar plates, the typical methodology used over the years for estimation of plaque-forming units (PFU) [e.g., Abedon and Yin (2009), Ellis and Delbruck (1939)]. Consistent with the confocal microscopy results, plate monitoring revealed a steep expansion phase that was proceeded by a gradual decrease in plaque size, with the final zone being approximately 50% of the maximal plaque area measured during the process (Fig 1B and C; Movie EV2). This plaque constriction occurrence was also evident when bacteria were infected with the distinct lytic phage Phi29 (Fig 1D), suggesting that such a kinetic pattern is widespread.

To concomitantly track plaque development and phage localization, we followed plaque formation by SPP1 harboring its lysin gene (*gp51*) fused to a yellow fluorescent protein (YFP) as a sole copy (SPP1-$_{\text{lysin-yfp}}$), marking active infection (Tzipilevich *et al*, 2017). Fluorescence from YFP demarcated the plaque periphery even during the constriction phase, signifying the presence of actively infected cells that release phage particles (Fig EV1A–C; Movie EV3). This observation implies that bacteria at the rim could withstand the presence of phages. Isolating bacteria from the edge of 30 different plaques subsequent to the constriction phase and re-plating them over plate-containing phages revealed all tested bacteria to remain phage sensitive (Fig EV1D). We refer to the phenomenon of phage-sensitive bacteria that can confront phages at the plaque circumference as "phage tolerance".

SigX is necessary for plaque constriction

The phenomenon of plaque constriction directed by phage-sensitive bacteria prompted us to postulate that bacteria residing at the plaque periphery could mount a transient phage tolerance response. We further reasoned that such a response could be orchestrated by one of the *B. subtilis* extracytoplasmic function (ECF) RNA polymerase sigma (σ) factors. These factors are activated in response to stress imposed on the cell envelope (Helmann, 2016) that could stem from remains of surrounding lysed cells. To examine this premise, we deleted each of the seven known ECF sigma factors of *B. subtilis* and assayed their impact on the final plaque size. Intriguingly, Δ*sigX* strain exhibited significantly larger plaques in comparison with wild-type (WT) when challenged with SPP1 or Phi29 phages (Fig 2A; Appendix Fig S1A). Furthermore, monitoring plaque dynamics revealed that this size difference is due to the substantial attenuation of the plaque constriction phase (Fig 2B and C). Importantly, when grown in liquid cultures, Δ*sigX* cells propagated with kinetics similar to that of WT cells (Appendix Fig S1B), indicating that the observed phenotype was not due to growth perturbation. To further elucidate the role of SigX in counteracting phage spread, we challenged Δ*sigX* cells with SPP1 or Phi29 phages in liquid cultures. No difference in lysis kinetics was observed when bacteria were infected at 1:1 (phage:bacteria) multiplicity of infection (MOI). However, while infected with low MOI (phage:bacteria, 1:20), Δ*sigX* cells lysed significantly faster than WT cells (Fig 2D; Appendix Fig S1C), a phenotype that could be reversed by ectopic expression of *sigX* (Appendix Fig S1D). The low MOI might be equivalent to the bacteria:phage ratio reached during the phase of plaque constriction. These results are consistent with the view that uninfected bacteria induce a SigX-regulated defense response, capable of tempering future phage infections.

To compare the response to phage attack of WT and Δ*sigX* cells in real time, we mixed mCherry-labeled WT cells with GFP-labeled Δ*sigX* cells and monitored plaque dynamics following infection with SPP1, utilizing time-lapse confocal microscopy. At the initial stages

Figure 1. Plaque formation dynamics reveals phases of expansion and constriction.

A BDR2637 (P_{veg}-*mCherry*) cells were infected with low concentrations (10^{-8} PFU/ml) of SPP1, placed on an agarose pad, and plaque formation was followed by time-lapse confocal microscopy. Shown are overlay images from mCherry signal (purple) and phase contrast (gray) of the bacterial lawn captured at the indicated time points (h). The plaque is seen as a hole formed on the bacterial lawn. Scale bar, 150 μm. Corresponds to Movie EV1.

B Plaque formation was monitored by automated scanning (Levin-Reisman *et al*, 2010) on a lawn of infected PY79 (WT) (10^{-6} PFU/ml) cells spread over an MB agar plate. Shown are images captured at the indicated time points (h). Scale bar, 2 mm. Corresponds to Movie EV2.

C, D The dynamic of SPP1 (C) and Phi29 (D) plaque formation following PY79 (WT) infection was monitored as described in (B). Shown is the diameter of individual plaques for each phage ($n \geq 12$), with the average highlighted in red.

Source data are available online for this figure.

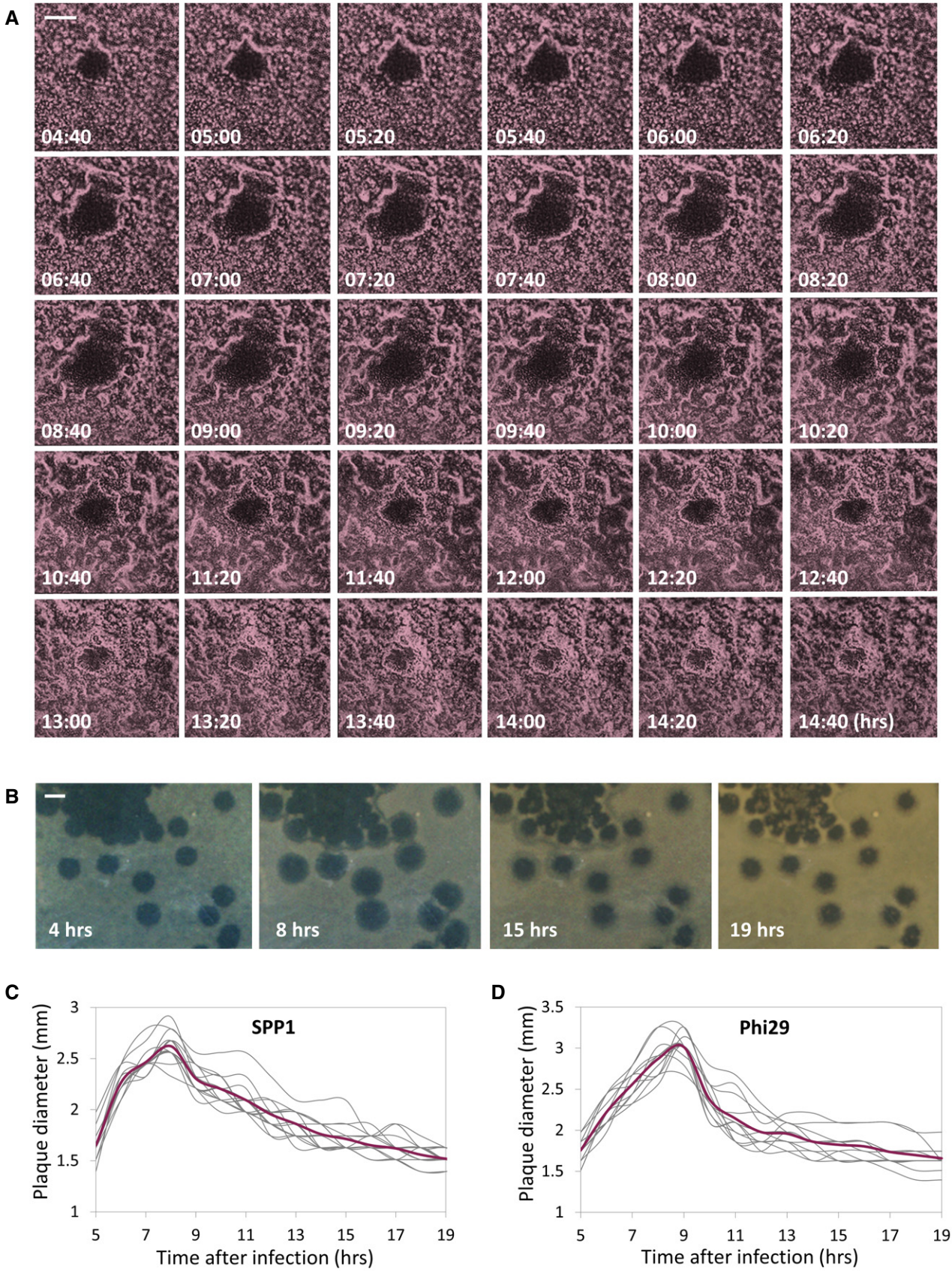
A
04:40
05:00
05:20
05:40
06:00
06:20
06:40
07:00
07:20
07:40
08:00
08:20
08:40
09:00
09:20
09:40
10:00
10:20
10:40
11:20
11:40
12:00
12:20
12:40
13:00
13:20
13:40
14:00
14:20
14:40 (hrs)
B
4 hrs
8 hrs
15 hrs
19 hrs
C
SPP1
Plaque diameter (mm)
Time after infection (hrs)
D
Phi29
Plaque diameter (mm)
Time after infection (hrs)

Figure 1.

of phage spreading, both strains appeared to be infected and to be lysed equally (Fig 2E, t = 5, 9 h; Appendix Fig S2A; Movie EV4). However, during the constriction phase, when the bacteria re-grew into the plaque zone, WT cells outcompeted the Δ*sigX* cells, as signified by the dominant colonization of the mCherry-labeled WT cells at the plaque rim (Fig 2E, t = 12, 16 h; Fig EV2; Appendix Fig S2A, Movie EV4). When GFP- and mCherry-labeled WT cells were mixed as a control, both strains were evenly distributed at the plaque edge even 16 hours postinfection (Fig EV2). Moreover, WT and Δ*sigX* cells equally occupied regions located remotely from visible plaque sites (Fig EV2), and, in accord, the growth rate of Δ*sigX* cells was not significantly affected by the presence of WT cells in a co-culture (Appendix Fig S2C). Consistent with these results, fusion of the *sigX* promoter to *gfp* (P_{sigX}-*gfp*) specified that cells located at the plaque rim produced GFP chiefly during the constriction phase (Fig 2F and Appendix Fig S2B). Interestingly, infection at 48°C, a temperature shown to activate *sigX* expression (Huang *et al*, 1997), led to a significant reduction in plaque size in a *sigX*-dependent manner (Fig EV3A). Of note, although no measurable difference between Δ*sigX* and WT growth kinetics was seen at 48°C (Fig EV3B), phage manufacture could be alleviated at high temperatures (Schachtele *et al*, 1970). In sum, we conclude that Δ*sigX* cells are deficient in inducing a defense mechanism that enables bacteria to tolerate the presence of phages and invade into the plaque zone.

SigX is activated in non-infected bacteria following infection of their neighbors

The results so far raised the prospect that bacteria could sense a danger signal, emanating from nearby infected bacteria, and in turn activate SigX-dependent phage tolerance response. To assay *sigX* induction in uninfected bacteria, SPP1 was added to WT cells that were co-cultured with SPP1-resistant bacteria, lacking the phage receptor (*ΔyueB*), and harboring the P_{sigX}-*gfp* reporter. Indeed, monitoring GFP fluorescence showed a continuous increase in *sigX* expression that reached the maximal level approximately 35 min postinfection and started to decline at t = 60 min (Figs 3A and EV3C and D). A similar fluorescence profile was obtained when the two strains were separated by a membrane that allows the passage of small molecules while compartmentalizing the cells (Fig 3B), suggesting that the *sigX*-inducing factor is secreted into the shared medium. To further substantiate the ability of bacteria to activate SigX in response to nearby infected cells, we followed the production and localization of SigX protein during infection at the cellular level. In the absence of phages, a functional SigX-GFP fusion (P_{sigX}-*sigX-gfp*) mainly localized onto the membrane, frequently forming focal assemblies in proximity to the cell circumference and at septal positions (Fig 3C and Appendix Fig S1E). This localization pattern is consistent with previous reports, showing that SigX is sequestered to the plasma membrane by its anti-sigma factor as a way to halt its action (Ho & Ellermeier, 2012). To assay SigX activity in uninfected bacteria, we added SPP1 phage to mCherry-labeled WT bacteria mixed with *ΔyueB* phage-resistant bacteria, harboring *sigX-gfp*. Time-lapse microscopy revealed repositioning of SigX-GFP from membrane and foci locations to massive nucleoid deployment in the resistant bacteria (Fig 3D; t = 35 min), indicating a switch from an inactive to an active mode. Noticeably, this shift in localization occurred prior to lysis of nearby infected sensitive bacteria and corresponded to the increase in P_{sigX}-GFP signal observed (Fig 3A and B). SigX-GFP level was dropped, and its localization into foci was largely restored in the resistant bacteria 95 min postinfection (Fig 3D), in line with the decline in *sigX* expression (Fig 3A and B), presumably corresponding to conclusion of the phage-sensing response. Taken together, SigX appears to be activated in phage-resistant bacteria upon sensing a danger signal from nearby infected sensitive cells. Notably, infecting *sigX-gfp*-sensitive cells with SPP1 showed that SigX-GFP largely displaces its position form the membrane to the nucleoid in the course of infection (Fig EV3E), denoting that also infected cells activate the SigX response.

Expression of SigX protects from phage infection

The impact of SigX on phage infection was further explored by constructing bacteria artificially expressing SigX under an IPTG-inducible promoter. Remarkably, expressing *sigX* prior to phage addition markedly attenuated both SPP1 and Phi29 infections, with the cells being capable of extending the infection process (Fig 4A). Next, mCherry-labeled cells, over-expressing SigX (P_{IPTG}-*sigX*), were incubated with non-labeled WT cells, and the mixture was infected with $SPP1_{-lysin\text{-}yfp}$. Consistent with the above observations, WT cells were rapidly infected and lysed, while cells over-expressing SigX appeared to be infected at slower kinetics and to a lesser extent (Fig 4B and C), a phenomenon that was also observed during infection with Phi29 (Fig EV4A).

Figure 2. SigX is required for plaque constriction.

A The indicated strains were infected with SPP1 (10^{-6} PFU/ml), spread over MB plates, and plaque diameter was monitored after 20 h of incubation. Shown is average plaque diameter and SD for each strain ($n \geq 54$).

B, C Plaque formation dynamic of SPP1 (B) and Phi29 (C) was monitored by automated scanning (Levin-Reisman *et al*, 2010) on a lawn of infected (10^{-6} PFU/ml) PY79 (WT) or ET19 (Δ*sigX*) cells spread over an MB agar plate. Shown are average values and SD from kinetic of random plaques for each strain ($n \geq 7$).

D PY79 (WT) and ET19 (Δ*sigX*) cells were infected with SPP1 at either high (phages:bacteria 1:1) or low (1:20) MOI, and OD_{600nm} was followed at 2-min intervals. Shown is a representative experiment out of 6 biological repeats, and the average values and SD of 8 technical repeats.

E BDR2637 (P_{veg}-*mCherry*) (WT, purple) and ET191 (P_{rrnE}-*gfp*, Δ*sigX*) (Δ*sigX*, cyan) cells were mixed, infected with low concentrations (10^{-8} PFU/ml) of SPP1, placed on an agarose pad, and plaque formation was followed by time-lapse confocal microscopy. Shown are overlay images from mCherry (purple) and GFP (cyan) signals of the bacterial lawn captured at the indicated time points (h). The plaque is seen as a hole formed on the bacterial lawn. Scale bar, 100 μm. Corresponds to Movie EV4.

F ET27 (P_{sigX}-*gfp*) cells were infected with low concentrations (10^{-8} PFU/ml) of SPP1, placed on an agarose pad, and plaque formation was followed by time-lapse confocal microscopy. Shown are fluorescence from GFP (upper panels) and corresponding phase contrast images (lower panels), captured at the indicated time points (h). The plaque is seen as a hole formed on the bacterial lawn. Scale bar, 100 μm.

Source data are available online for this figure.

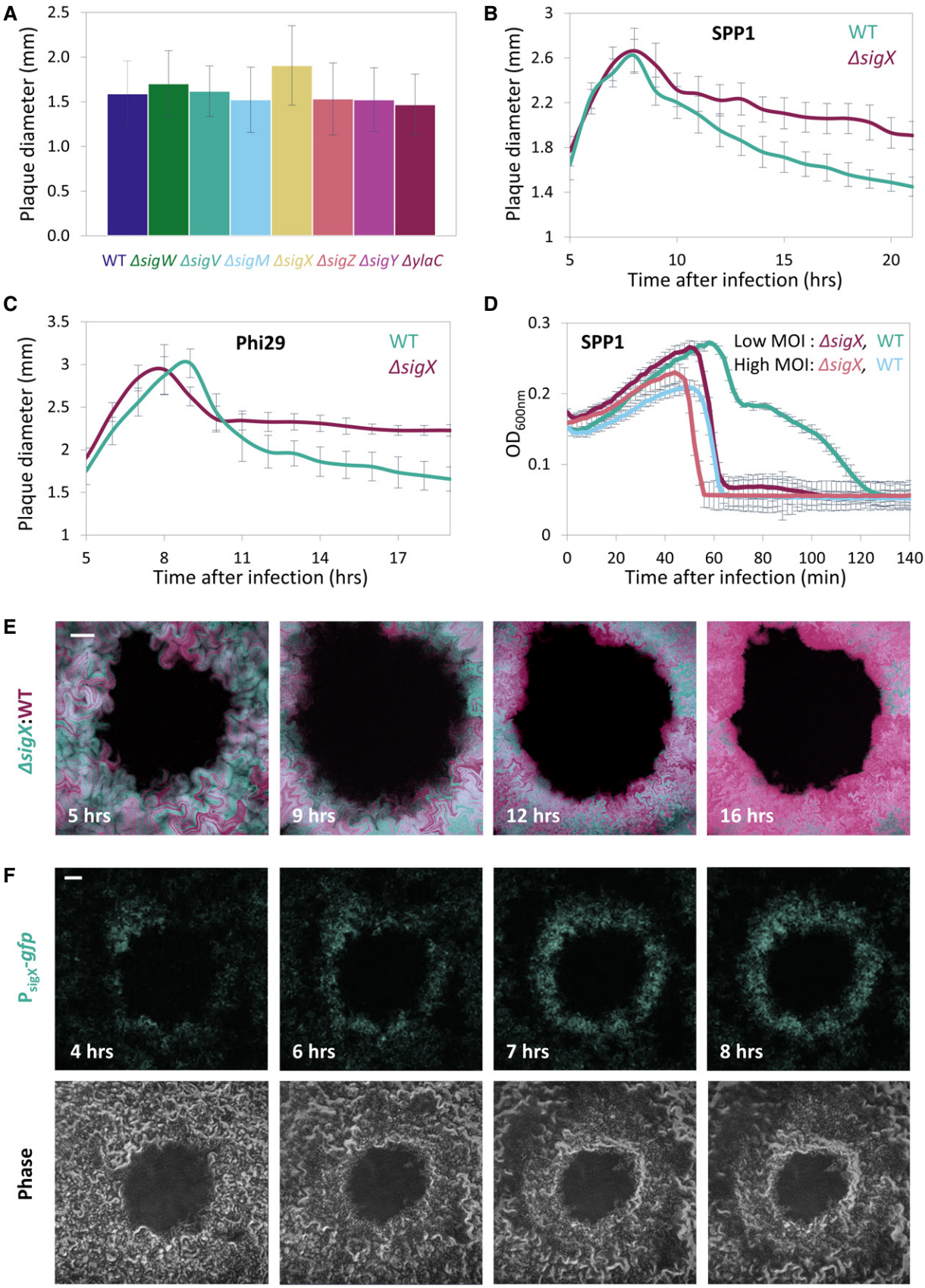
A
Plaque diameter (mm)
2.5
2.0
1.5
1.0
0.5
0.0
WT ΔsigW ΔsigV ΔsigM ΔsigX ΔsigZ ΔsigY ΔylaC
B
SPP1
WT
ΔsigX
Plaque diameter (mm)
3
2.6
2.2
1.8
1.4
1
5
10
15
20
Time after infection (hrs)
C
Phi29
WT
ΔsigX
Plaque diameter (mm)
3.5
3
2.5
2
1.5
1
5
8
11
14
17
Time after infection (hrs)
D
SPP1
Low MOI : ΔsigX, WT
High MOI: ΔsigX, WT
OD600nm
0.3
0.2
0.1
0
0
20
40
60
80
100
120
140
Time after infection (min)
E
ΔsigX:WT
5 hrs
9 hrs
12 hrs
16 hrs
F
PsigX-gfp
4 hrs
6 hrs
7 hrs
8 hrs
Phase

Figure 2.

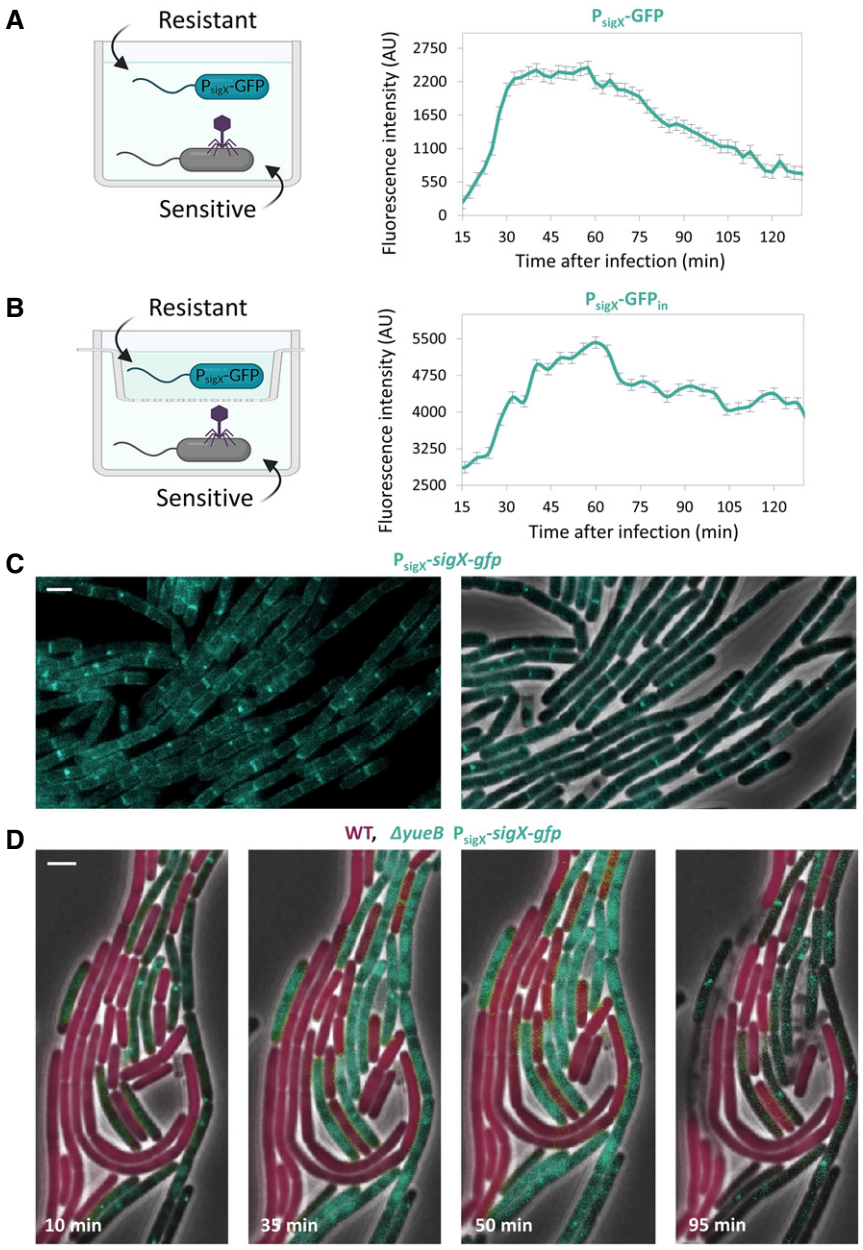

Figure 3. SigX is activated in non-infected cells upon infection of their neighbors.

A Phage-sensitive PY79 (WT) cells were mixed with phage-resistant BS12 (Δ*yueB*, P_{sigX}-*gfp*) cells and the mixture was infected with SPP1, as illustrated. Infection was conducted at 2:1 (phages:bacteria) MOI, and fluorescence intensity from P_{sigX}-*gfp* (AU) was followed at 2.5-min intervals. Uninfected mixed population served as a control, and its fluorescence was subtracted from the overall GFP signal of the infected culture. Shown is a representative experiment out of 3 biological repeats, and the average values and SD of 8 technical repeats.

B Phage-sensitive PY79 (WT) cells were infected with SPP1 at 2:1 (phages:bacteria) MOI, and placed in the outer ring of a transwell, as illustrated. Phage-resistant BS12 (Δ*yueB*, P_{sigX}-*gfp*) were placed in the inner ring. Fluorescence intensity from P_{sigX}-*gfp* (AU) of the inner compartment was followed at 2.5-min intervals. Uninfected population served as a control, and its fluorescence was subtracted from the overall GFP signal of the infected culture. Shown is a representative experiment out of 3 biological repeats, and the average values and SD of 8 technical repeats.

C ET26 (P_{sigX}-*sigX-gfp*) cells were visualized by fluorescence microscopy. Shown are signal from SigX-GFP (cyan) (left panel), and an overlay image of phase contrast (gray) and signal from SigX-GFP (cyan) (right panel). Scale bar, 1 μm.

D BDR2637 (P_{veg}-*mCherry*) (WT, purple) and ET261 (Δ*yueB*, P_{sigX}-*sigX-gfp*) (cyan) cells were mixed, infected with SPP1 at 5:1 (phages:bacteria) MOI, placed on an agarose pad, and followed by time-lapse fluorescence microscopy. Shown are overlay images from mCherry (purple), SigX-GFP (cyan), and phase contrast (gray), captured at the indicated time points postinfection. Scale bar, 1 μm.

Source data are available online for this figure.

To define the specific stage at which phage infection was interrupted by SigX activity, we followed the adsorption of phages to cells over-expressing *sigX*. A standard adsorption assay yielded no significant difference in SPP1 adsorption rate between WT and SigX expressing cells (Fig 4D). Nonetheless, since SPP1 phage exhibits two modes of cell surface binding, reversible in which it associates with gWTA polymers, and irreversible, through interaction with the YueB receptor (Baptista *et al*, 2008), it was still conceivable that the irreversible mode of binding was impaired. To inspect this possibility, cells were diluted after an initial phage adsorption period to enable reversibly adsorbed phages to detach from the host (Baptista *et al*, 2008). Indeed, a large fraction of phages, adsorbed to *sigX* over-expressing cells, were liberated after dilution, whereas no significant release of WT-attached phages was detected (Fig 4D), indicating that SigX expression delays SPP1 irreversible binding. To corroborate this finding, we investigated whether phage DNA injection is consequently delayed by induced expression of SigX. To monitor phage DNA injection, we utilized SPP1-$_{delX110lacO64}$ phage, which contains 64 repeats of *lacO* (Jakutyte *et al*, 2012), and infected bacteria chromosomally expressing *lacI-cfp*. The presence of phage DNA within the host cytoplasm was visualized subsequent to injection by the formation of LacI-CFP foci (Fernandes *et al*, 2016; Tzipilevich *et al*, 2017). Infection of WT cells resulted in foci appearance within 10 min after infection, while no foci were observed in *sigX* over-expressing cells at the same time point (Fig 4E and F), indicating a delay in phage DNA penetration into the latter cell population. Consistent with this possibility, a significant decrease in SPP1-mediated plasmid transduction rate into SigX-producing cells was monitored (Fig EV4B). Thus, we surmise that *sigX* expression interferes with SPP1 irreversible binding and consequently delays phage DNA injection.

The *dlt* operon mediates the SigX tolerance response to phage infection

To identify the gene(s) required for SigX-mediated phage tolerance, we mutated known genes in the SigX regulon (Huang & Helmann, 1998) and tested their impact on the phage protection phenotypes. Out of the mutants tested, only the disruption of *ywbO*, encoding a predicted disulfide oxidoreductase, and that of the *dlt* operon (Δ*dltA*), largely countered the tolerance to phage infection conferred by SigX over-expression (Figs 5A and EV5A). The *dlt* operon encodes an enzymatic pathway that is known to ligate D-alanine moieties to TA polymers (Perego *et al*, 1995), the major phage surface attachment components, and was therefore selected for further investigation. Examination of infected *ΔdltA* mutant cells harboring inducible *sigX* by fluorescence microscopy substantiated that they were lysed with kinetics similar to that of WT cells in the presence of the inducer (Fig EV5B). Furthermore, deletion of *dltA* restored the capacity of SPP1 to bind irreversibly to the surface of *sigX* over-expressing cells, and consistently increased the level of SPP1 DNA injection into these cells, as detected by transduction assay (Fig 5B and C). Lastly, deletion of *dltA,* in an otherwise WT background, resulted in enhanced sensitivity to infection at low MOI, whereas over-expression of the *dlt* operon could increase resistance to phages compared to WT (Fig EV5C and D).

To substantiate the role of the *dlt* operon in the phage tolerance response, we examined the phenotype of Δ*dltA* during plaque generation. Δ*dltA* cells exhibited plaques larger than that of the WT, along with prominent deficiency in plaque constriction phase (Fig 5D and E), similar phenotypes to those observed for the Δ*sigX* cells (Fig 2A and B). Next, we mixed differentially labeled Δ*dltA* and WT cells, and followed plaque formation dynamics by time-lapse confocal microscopy. While the two populations were evenly distributed at early stages of plaque generation, WT cells were manifestly dominating the plaque rim during constriction (Fig 5F and Appendix Fig S3A), indicating a clear deficiency of the mutant cells in opposing infection. Monitoring DltA expression by following DltA-YFP showed an enrichment of the fusion protein preferentially at the edge of the constricting plaque (Fig 5G and Appendix Fig S3B), supporting a role in mediating this process. In sum, the majority of the phage protection phenotypes conferenced by SigX can be assigned to the *dlt* operon, encoding enzymes that modify the TA surface polymers.

Figure 4. SigX expression confers phage tolerance.

A PY79 (WT) and ET28 (P_{IPTG}-*sigX*) cells were infected with SPP1 or Phi29 (t = 60 min) at 1:20 (phages:bacteria) MOI, and OD_{600nm} was followed at 2-min intervals. IPTG was added 30 min before infection (t = 30 min). Shown is a representative experiment out of 3 biological repeats, and the average values and SD of 4 technical repeats.

B ET29 (P_{veg}-*mCherry*, P_{IPTG}-*sigX*) (purple) cells were grown in the presence of IPTG and mixed with PY79 (WT) cells. The mixture was infected with SPP1-$_{lysin\text{-}yfp}$ 5:1 (phages:bacteria) MOI, placed on an IPTG-containing agarose pad, and followed by time-lapse fluorescence microscopy. Shown are overlay images of phase contrast (gray), signal from mCherry-labeled cells (purple), and signal from Lysin-$_{SPP1}$-YFP (cyan), captured at the indicated time points postinfection (upper panels). Corresponding signal from Lysin-$_{SPP1}$-YFP (cyan) is shown separately (lower panels). Arrows highlight the delayed infection of ET29 cells. Scale bar, 1 μm.

C Quantification of the experiment described in (B). Shown is the percentage of phage infected PY79 (WT) and ET29 (P_{veg}-*mCherry*, P_{IPTG}-*sigX*) cells at the indicated time points, scored by the Lysin-$_{SPP1}$-YFP signal, with average values and SD ($n \geq 200$ cells for each time point). Of note, the majority of WT cells were lysed at t = 75 min postinfection.

D PY79 (WT) and ET28 (P_{IPTG}-*sigX*) cells, grown in the presence or absence of IPTG, were infected with SPP1 (1:1 MOI) for 10 min. Next, phage adsorption was monitored before and after cell dilution (×100 fold). Percentage of phage adsorption was calculated as follows: $(P_0 - P_1) \times 100/P_0$, where P_0 is the initial phage input in the lysate (PFU/ml), and P_1 is the titer of free phages (PFU/ml) 10 min after infection. Shown are average values and SD of a representative experiment out of 3 independent experiments.

E OF83 (P_{pen}-*lacIΔ11-cfp*) (WT) and ET40 (P_{pen}-*lacIΔ11-cfp*, P_{IPTG}-*sigX*) cells, grown in the presence or absence of IPTG, were infected with SPP1-$_{delX110lacO64}$ at 5:1 (phages:bacteria) MOI. The formation of LacI-CFP foci on phage DNA was monitored 10 min postinfection. Non-infected OF83 cells were used for comparison. Shown are overlay images of phase contrast (gray) and signal from LacI-CFP (cyan). Scale bar, 1 μm.

F Quantification of the experiment described in (E). Shown is the percentage of LacI-CFP foci 10 min postinfection of OF83 and ET40 cells by SPP1, with average values and SD ($n \geq 850$ cells for each population). This is a representative experiment out of 3 biological repeats.

Source data are available online for this figure.

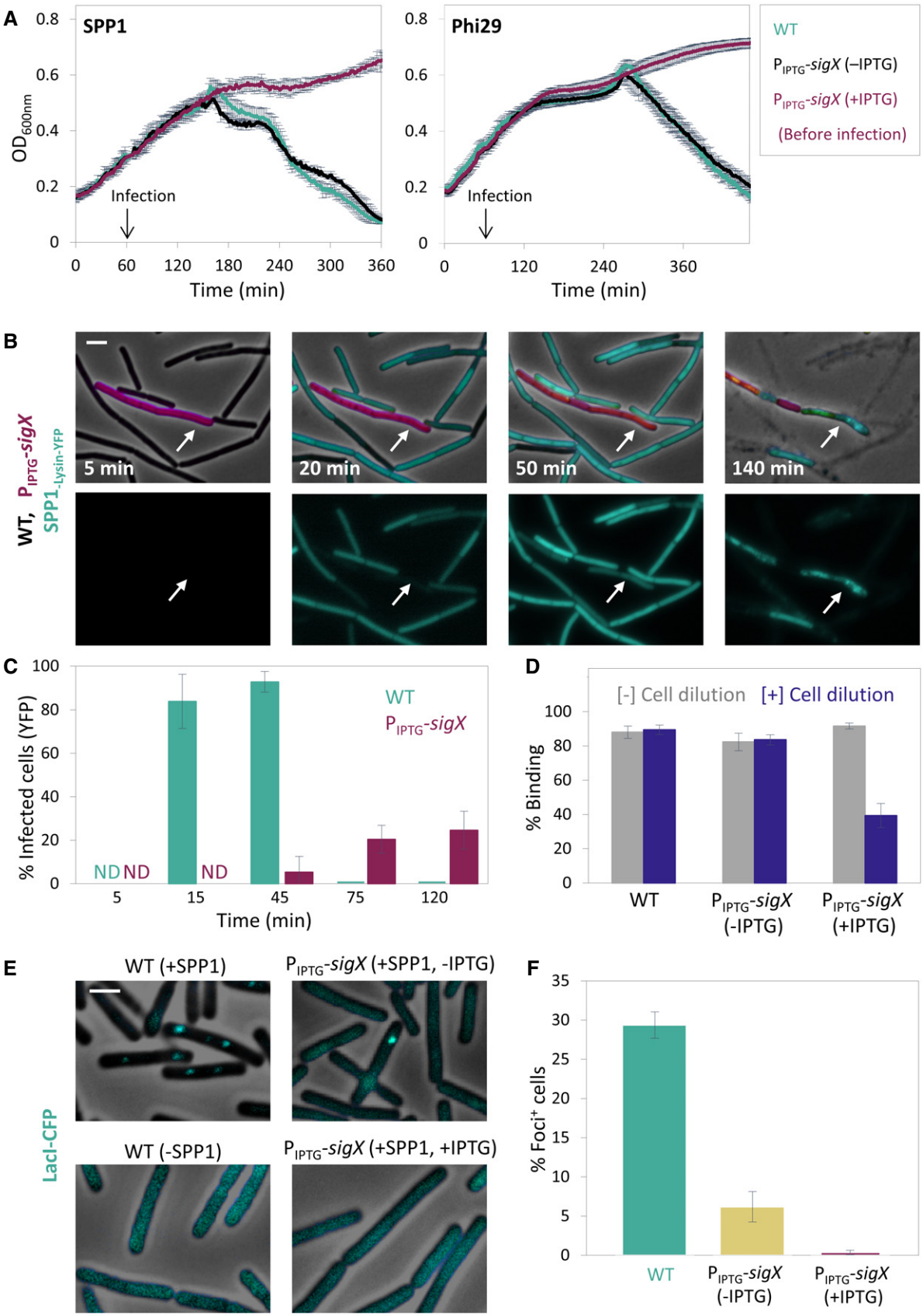

Figure 4.

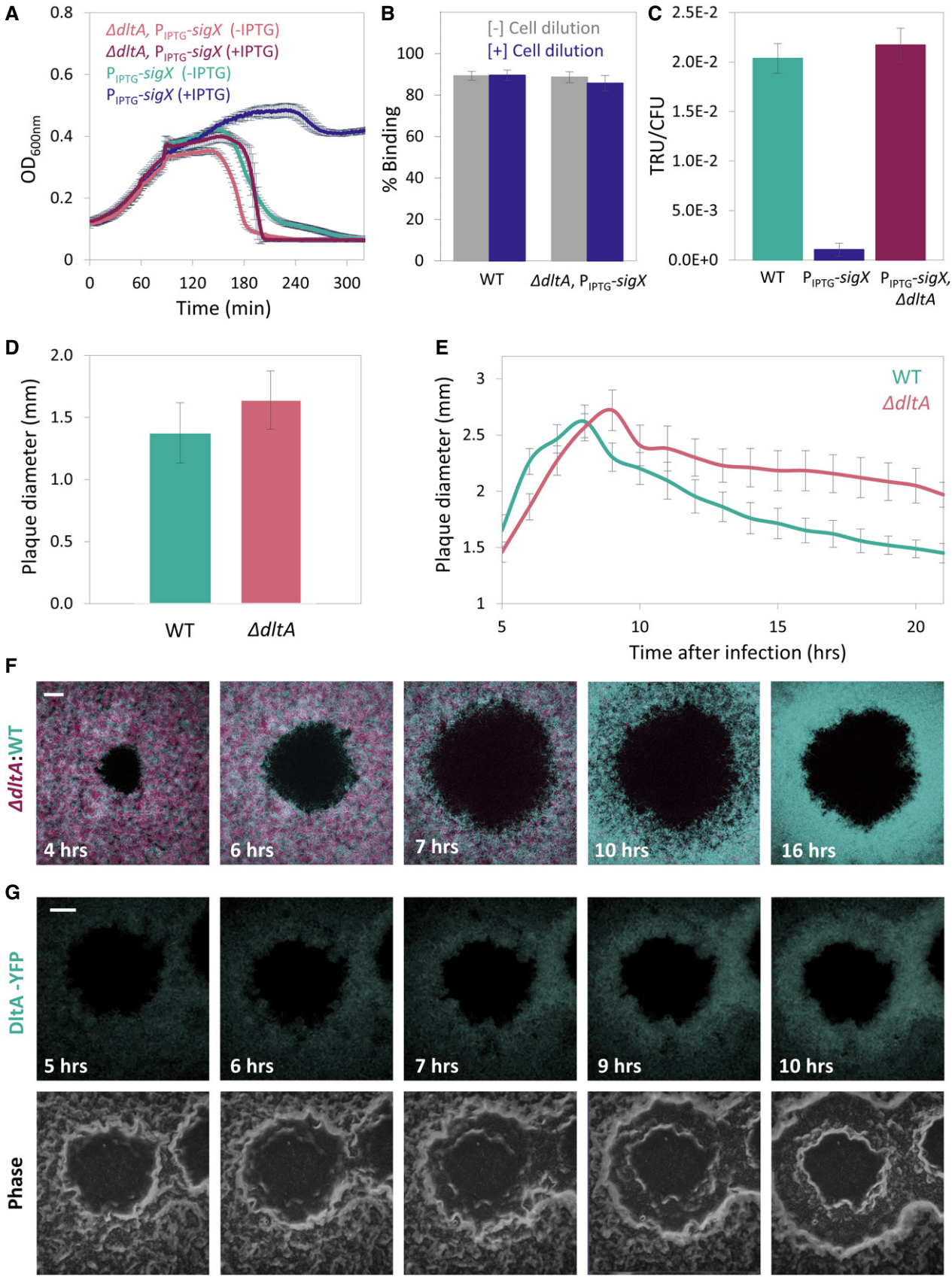

Figure 5.

Figure 5. The *dlt* operon mediates the SigX-induced phage tolerance response.

A ET28 (P_{IPTG}-*sigX*) and ET42 (Δ*dltA*, P_{IPTG}-*sigX*) cells, grown in the presence or absence of IPTG, were infected with SPP1 at 1:20 (phages:bacteria) MOI, and OD_{600nm} was followed at 2-min intervals. Shown is a representative experiment out of 6 biological repeats, with the average values and SD of 8 technical repeats.

B PY79 (WT) and ET42 (*ΔdltA*, P_{IPTG}-*sigX*) cells, grown in the presence of IPTG, were infected with SPP1 (1:1 MOI) for 10 min. Next, phage adsorption was monitored before and after cell dilution (×100-fold). Percentage of phage adsorption was calculated as follows: $(P_0-P_1) \times 100/P_0$, where P_0 is the initial phage input in the lysate (PFU/ml), and P_1 is the titer of free phages (PFU/ml) 10 min after infection. Shown are average values and SD of 5 biological repeats.

C PY79 (WT), ET28 (P_{IPTG}-*sigX*), and ET42 (*ΔdltA*, P_{IPTG}-*sigX*), grown in the presence of IPTG, were transduced with SPP1-pBT163 lysate, and the number of transductants was monitored by plating the cells on selective plates. Transduction unit (TRU) was calculated as the number of transductant colonies /total colony-forming unit (CFU). Shown are average values and SD of 3 biological repeats.

D PY79 (WT) and ET41 (*ΔdltA*) cells were infected with SPP1 (10^{-6} PFU/ml), spread over an MB agar plate, and plaque diameter was monitored after 20 h of incubation. Shown is plaque diameter distributions for each strain ($n \geq 40$).

E Plaque formation dynamic of SPP1 was monitored by automated scanning (Levin-Reisman *et al*, 2010) on a lawn of infected (10^{-6} PFU/ml) PY79 (WT) or ET41 (*ΔdltA*) cells grown on an MB agar plate. Shown are average values and SD from kinetics random plaques for each strain ($n \geq 10$).

F AR16 (P_{rrnE}-*gfp*) (WT, cyan) and ET411 (P_{veg}-*mCherry*, Δ*dltA*) (Δ*dltA*, purple) cells were mixed, infected with low concentrations (10^{-8} PFU/ml) of SPP1, placed on an agarose pad, and plaque formation was followed by time-lapse confocal microscopy. Shown are overlay images from GFP (cyan) and mCherry (purple) signals of the bacterial lawn captured at the indicated time points (h). The plaque is seen as a hole formed on the bacterial lawn. Scale bar, 150 μm.

G ET43 (*dltA-yfp)* cells were infected with low concentrations (10^{-8} PFU/ml) of SPP1, placed on an agarose pad, and plaque formation was followed by time-lapse confocal microscopy. Shown are fluoresce from DltA-YFP signal (upper panels) and corresponding phase contrast images (lower panels), captured at the indicated time points (h). The plaque is seen as a hole formed on the bacterial lawn. Scale bar, 100 μm.

Source data are available online for this figure.

Discussion

By following the dynamics of plaque formation on lawns of the soil bacterium *B. subtilis,* we discovered that plaque development includes a phase of constriction, typified by bacterial growth into the plaque zone, counteracting plaque expansion. Examination of bacteria located at the plaque rim subsequent to constriction revealed that they are not genetically resistant to phages, but instead elicit a temporary phage tolerance response, activated by the stress-induced RNA polymerase sigma factor σ^X. We further uncovered that the impact of SigX on tolerance is not restricted to plaques, as uninfected bacteria activated *sigX* expression following infection of their neighbors in a co-culture. Furthermore, pre-expression of *sigX* prior to phage addition was found to protect from phage attack. SigX tolerance is mostly attributed to the action of the *dlt* operon, encoding for WTA modifying enzymes, thereby altering the polymer properties. Based on our results, we propose that uninfected bacteria can sense infection of their neighbors, and in turn trigger a tolerance response, modifying their phage attachment surface components to antagonize phage penetration (Fig 6). As such, the cells at the plaque rim form a protective barrier that locally constrains plaque spread, shielding the non-infected population.

This scenario resembles the eukaryotic innate immune response, with the hallmark being interferon released by infected cells and received by neighbors to activate an anti-viral response (Isaacs & Lindenmann, 1957; McNab *et al*, 2015). In addition, endogenous danger signals, such as extracellular ATP and DNA, released by infected eukaryotic cells, stimulate innate immunity (Gallucci & Matzinger, 2001), a program that could be applicable for activating the phage tolerance response. Importantly, damaged-self recognition stimulated by similar factors exists in plants and even in algae and fungi (Heil & Land, 2014). Interestingly, it has been shown that bacteria possess the cyclic GMP–AMP synthase (cGAS)–STING pathway, a central component of the mammalian innate immune system, as part of an anti-phage defense mechanism (Cohen *et al*, 2019; Morehouse *et al*, 2020). The observation that *sigX* expression in non-infected bacteria can be stimulated by compartmentally separated infected cells suggests that the signaling factor is a small molecule, capable of passing thought a small sized pore. Such molecule might determine a threshold level required for robust and efficient activation of the tolerance response seen during advanced stages of plaque development. The effectiveness of tolerance was also MOI-dependent, suggesting that phage to bacteria ratio at the plaque rim decreases eventually to allow a powerful response. It is thus possible that phages exhibiting large burst size are more adapted to antagonize tolerance.

Our data indicate that bacteria acquire phage tolerance chiefly by remodeling their cell surface, decorating WTA polymers with D-alanine residues (Brown *et al*, 2013). D-alanylation of TA polymers is executed by a series of chemical reactions performed by the Dlt enzymes (Perego *et al*, 1995; Percy & Grundling, 2014; Ma *et al*, 2018). It has been shown that TA D-alanylation contributes to resistance against cationic antimicrobial peptides and lysozyme (Kovacs *et al*, 2006; Kingston *et al*, 2013), presumably due to changes in the cell surface electric charge or increase in peptidoglycan density (Saar-Dover *et al*, 2012; Percy & Grundling, 2014). D-alanylation of TA was also shown to enhance host cell adhesion and virulence of Gram-positive pathogens such as *Staphylococcus aureus* and *B. anthracis* (Simanski *et al*, 2013; Percy & Grundling, 2014). Since TA glycosylation is known to serve as a pervasive phage binding molecule (Young, 1967; Habusha *et al*, 2019), it is plausible that WTA-D-alanylation masks WTA glycosylated sites, and/or interferes with bacteriophage access to the membrane. Notably, apart from the *dlt* operon, *ywbO* appears to contribute to phage tolerance. Recently, mutations in *ywbO* promoter region were linked to impediment in TA glycosylation, pointing at an additional path through which phage tolerance by surface modulation might be achieved (Tzipilevich & Benfey, 2021).

The induction of the phage tolerance response was shown to be mediated by SigX, belonging to the ECF family that monitors cell wall integrity. SigX is recruited to the membrane by its cognate anti-sigma factor and is liberated to the nucleoid in response to envelope stress to transcribe downstream target genes, with one of the most

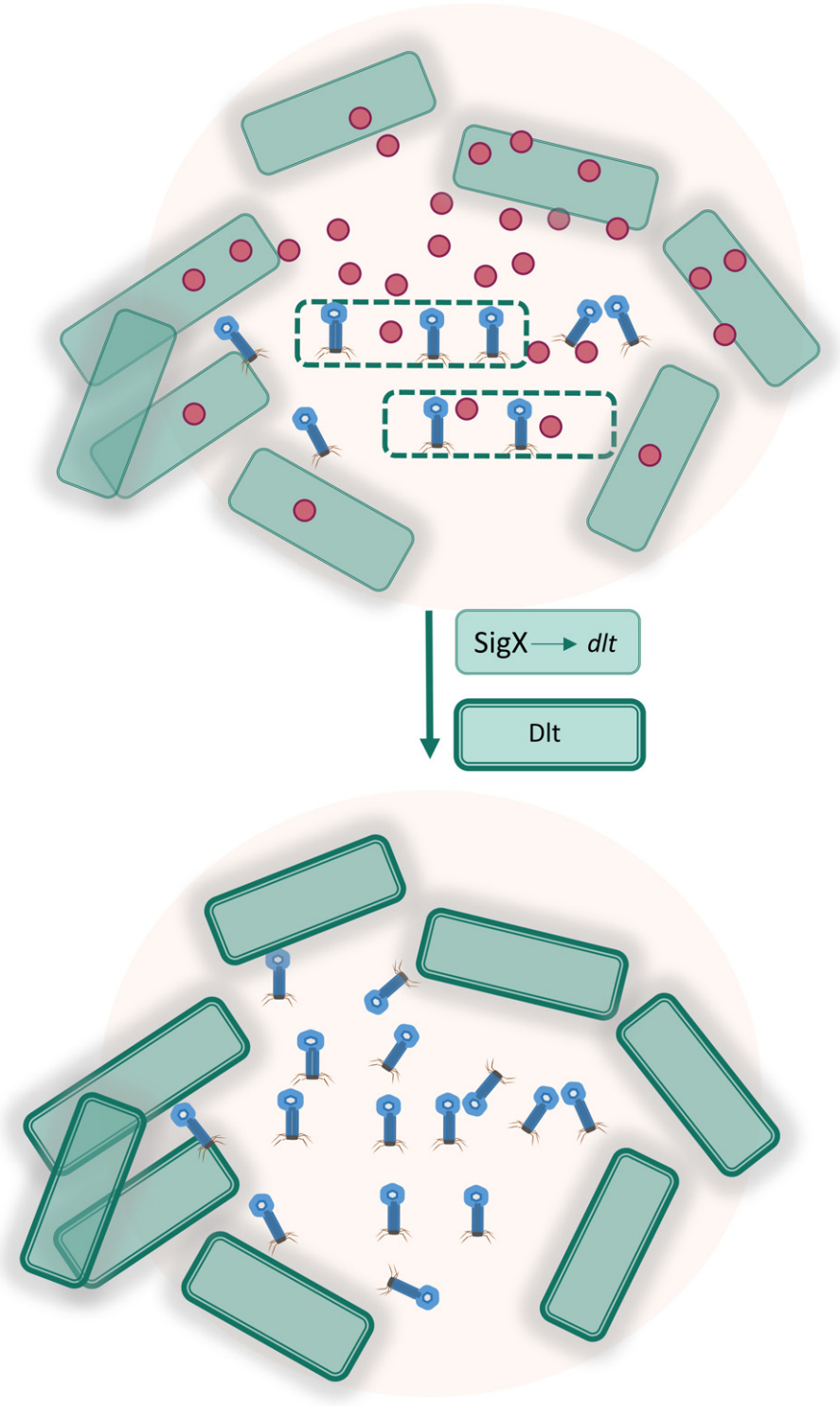

Figure 6. A model for eliciting phage tolerance response by uninfected bacteria.

Upon phage infection, bacteria (dashed-line cells) generate a yet unidentified "danger signal" (red circles) that is received by uninfected neighboring cells. In turn, the latter cells activate SigX that induces the transcription of the *dlt* operon. The produced Dlt enzymes modulate the phage receptor WTA polymers to reduce phage binding, providing temporary protection against phage attack and limiting phage spread.

prominent being the *dlt* operon (Cao & Helmann, 2004; Helmann, 2016). A *sigX* mutant strain was shown to be sensitive to heat and oxidative stress, and to be susceptible to cationic antimicrobial peptide (Huang *et al*, 1997; Cao & Helmann, 2004). Indeed, we found that elevated growth temperature seems to protect bacteria from phage attack in a SigX-dependent manner, hinting that cross-activation of ECF enables bacteria to simultaneously resist multiple stress conditions, similarly to SOS response (Storz, 2016; Gottesman, 2019). Still, the nature of the activating signals and how they are transduced to release the membrane-attached SigX have yet to be elucidated. Since ECFs are widespread among bacteria (Helmann, 2002), it is tempting to assume that, similarly to *B. subtilis*, many species have the capacity to execute such a defense strategy, following infection of nearby bacteria. We postulate that such phage tolerance might expedite the acquisition of permanent phage resistance mutations in nature, similarly to tolerance to antibiotic stress that facilitates emergence of antibiotic resistance mutants (Liu *et al*, 2020).

Bacteria have evolved numerous remarkable phage resistance strategies to counteract infection, including restriction-modification systems, abortive infection, CRISPR-Cas immunity (Labrie *et al*, 2010; Salmond & Fineran, 2015), and a plethora of recently identified additional exciting systems [e.g., Cohen *et al* (2019), Doron *et al* (2018), Gao *et al* (2020), Makarova *et al* (2011)]. Still, relatively little is known about the dynamics of the activation of these systems within populations. For instance, it is not entirely understood how activation of the various CRISPR-Cas systems is prompted. There is evidence for constitutive activity of *Cas* genes in some bacteria, and for quorum sensing-mediated transcription of *Cas* genes in others (Patterson *et al*, 2017; Hampton *et al*, 2020). Consistently, proteomic analysis revealed that phage infection elevates Cas production in *Streptococcus thermophilus* (Young *et al*, 2012). Knowledge concerning population dynamics of other phage defense systems is even more fragmentary. Here, we uncovered a general phage tolerance mechanism that provides only temporary protection by phenotypic modulation of the bacterial cell surface. To the best of our knowledge, this is the first detailed characterization of a phage defense system in space and time.

Materials and Methods

Strains and plasmids

Bacillus subtilis strains were derivatives of the wild-type PY79 (Youngman *et al*, 1984). All bacterial strains and phages are listed in Appendix Table S1. Plasmid constructions were performed in *E. coli* DH5α using standard methods and are listed in Appendix Table S1. All primers used in this study are listed in Appendix Table S2.

General growth conditions

Bacterial cultures were inoculated at OD_{600nm} 0.05 from an overnight culture and growth was carried out at 37°C, unless indicated otherwise, in LB medium supplemented with 5 mM $MgCl_2$ and 0.5 mM $MnCl_2$ (MB). Fluorescence measurement experiments in plate reader were conducted in CH (10% casein hydrolysate) medium supplemented with 5 mM $MgCl_2$ and 0.5 mM $MnCl_2$ (Harwood & Cutting, 1990). For induction, all $P_{hyper\text{-}spank}$ controlled genes were induced with isopropyl-β-D-thiogalactopyranoside (IPTG) at concentration of 0.5 mM.

General phage infection and transduction methodologies

Phage lysate was prepared by adding approximately 10^9 phages to 1 ml mid-log cells grown in MB until the culture was completely cleared. Next, the lysate was filtered through 0.45-μm or 0.22-μm Millipore filter. For lysis dynamic experiments, phages were added to mid-log growing cells at the indicated MOI, and OD_{600nm} was monitored. For SigX-induction experiments, cells were grown for 30 min in the absence of inducer. Subsequently, inducer was added and cells were grown for additional 30 min. Phages were added after overall growth of 60 min, and OD_{600nm} was followed by Spark 10M (Tecan) multiwell fluorometer set at 37°C with a constant shaking.

For transduction experiments, lysates were prepared from a given donor strain as describe above. All lysates for transduction were treated with DNase I (Sigma-Aldrich) 200 ng/ml for 20 min at RT. Recipient strains were grown to 1.0 OD_{600nm}, and cells (1 ml) were mixed with 100 μl of lysate and 9 ml of MB, and incubated at 37°C without shaking for 20 min. Subsequently, cells were centrifuged and spread on selective plates supplemented with 10 mM sodium citrate. For burst size measurement, $1{:}10^4$ phages:bacteria were added to a mid-log culture, and 30 min later, the culture was lysed with chloroform and the number of phages in the culture was measured.

Phage attachment assay

Indicated bacterial strains were grown in a liquid culture to 0.6 $OD_{600\ nm}$, and phage adsorption to the cells was measured at 10 min postinfection, by titrating the free phages present in the supernatant as previously described (Ellis & Delbruck, 1939). In brief, logarithmic cells were grown in MB at 37°C till 0.8 OD_{600nm}; then, 15 mM $CaCl_2$ and 50 μg chloramphenicol/ml were added to the medium and cells were incubated for 10 min. Next, cells were infected with phages (10^7 PFU/ml), and samples (0.5 ml) were collected at 10 min postinfection and centrifuged for 1 min, and 50 μl of the supernatant was diluted and plated, and PFU/ml was determined. To measure reversible attachment, 10 min postinfection, cells were diluted 100 fold in fresh MB and incubated for 2 min in 37°C, and free phages present in the supernatant were plated and PFU/ml was determined.

Plaque size determination

For final plaque size determination, bacteria from mid-log culture were infected with low concentration of phages (10^{-6} PFU/ml) and spread over 1.5% MB agar plates at 37°C or 48°C for 20 h. Next, plates were photographed and plaque size was determined by measuring the size of random plaques. Image processing was performed using MetaMorph 7.4 software (Molecular Devices). For analyzing plaque growth dynamics on agarose plates, bacteria were infected as describe above, and 1.5% MB agar plates were incubated at 37°C on top of a scanner and covered with a dark paper cover. An automated scanning program (Levin-Reisman *et al*, 2010) was utilized for time-lapse imaging of the plates. Plaque size was

determined by measuring the size of random plaques at intervals of 1 h. Image processing was performed using MetaMorph 7.4 software (Molecular Devices).

Fluorescence microscopy

For fluorescence microscopy, bacterial cells (0.5 ml, OD_{600nm} 0.5) were centrifuged and suspended in 50 μl of MB. For time-lapse microscopy, bacteria were placed over 1.5% MB agarose pad and incubated in a temperature controlled chamber at 37°C. Infection experiments were carried out at 5:1 (phages:bacteria) MOI. Samples were photographed using Axio Observer Z1 (Zeiss) or Eclipse Ti microscope (Nikon, Japan), equipped with CoolSnap HQII camera (Photometrics, Roper Scientific, USA). System control and image processing were performed using MetaMorph 7.4 software (Molecular Devices) or NIS Elements AR 4.3 (Nikon, Japan).

Live imaging of developing plaques by confocal microscopy

A custom designed construct (Mamou *et al*, 2016) was used to monitor bacterial plaques by confocal microscopy. Accordingly, a 40-mm metal ring was filled with 1.5% MB agarose and assembled, and the bacterial cells were infected at low MOI (10^{-8} PFU/ml) and spotted over the agarose pad. Plaque growth construct was covered with a 35-mm cultFoil membrane (Pecon) to reduce agar dehydration and incubated in Lab-Tek S1 heating insert (Pecon) placed inside an incubator XL-LSM 710 S1 (Pecon). Initial plaques could be observed under the microscope at $t = 4$ h. Developing plaques were visualized and photographed by CLSM LSM700 (Zeiss). Cells expressing GFP or YFP were irradiated using 488 nm laser beam, while mCherry-expressing cells were irradiated using 555 nm laser beam. For each experiment, both transmitted and reflected light were collected from 6 consecutive Z positions by 10-μm steps. System control, image processing, and fluorescence quantifications were carried using Zen software version 5.5 (Zeiss).

Fluorescence intensity measurements by a plate reader

For continuous measurements of fluorescence intensity and OD_{600nm}, cells were grown in CH (due to a low background fluorescence of the medium), at 37°C until 0.2-0.5 OD_{600nm}, and infected with SPP1 or Phi29. Fluorescence intensity (AU) and OD_{600nm} were measured by Spark 10M (Tecan) multiwell fluorometer plate reader every 2/2.5 min at 37°C with constant shaking. A 12-well Transwell Permeable Supports plates with 12-mm-diameter inserts was used for the transwell assay. In transwell experiments, sensitive and resistant cells were separated by a 0.4-μm polycarbonate membrane. The plate was read either at a setting to read the full well or only the center (insert). OD_{600nm} cannot be faithfully read by Spark 10M in transwells due to light distortion. Thus, for transwell experiments, samples were tested for OD_{600nm} in a spectrophotometer.

Statistical analysis

Unless stated otherwise, bar charts and graphs display a mean ± SD from at least 3 repeats. Quantifications of CPU, PFU, and infected cells were done manually. MS Excel was used for all statistical analysis, data processing, and presentation.

Data availability

There are no public datasets associated with the results presented in this manuscript.

Expanded View for this article is available online.

Acknowledgments

We thank R. Losick (Harvard University, USA), I. Rosenshine and A. Rouvinski (Hebrew University, Israel), and members of the Ben-Yehuda laboratory for valuable discussions. We thank N. Balaban and her laboratory members (Hebrew University, Israel) for assistance with the automated plaque scanning procedure. We are grateful to P. Tavers (Gif-sur-Yvette, France), J. Helmann (Cornell University, USA), and D. Rudner (Harvard University, USA) for providing strains. Artwork in Fig 3 and synopsis was prepared using BioRender (Agreement Number II2338U308, CN2368MHCR). This work was supported by the NSF/BSF-United States-Israel Binational Science Foundation (2017672), and the ERC Synergy grant (810186) awarded to S. B.-Y.

Author contributions

ET and OPF involved in conception and design, acquisition, analysis, interpretation of data, writing, and revising the article; BS performed acquisition of data, interpretation and analysis of data, and revising the article; and SBY performed conception and design, analysis and interpretation of data, writing and revising the article, supervision, and funding.

Conflict of interest

The authors declare that they have no conflict of interest.

References

Abedon ST, Yin J (2009) Bacteriophage plaques: theory and analysis. *Methods Mol Biol* 501: 161 – 174

Alonso JC, Luder G, Stiege AC, Chai S, Weise F, Trautner TA (1997) The complete nucleotide sequence and functional organization of *Bacillus subtilis* bacteriophage SPP1. *Gene* 204: 201 – 212

Baptista C, Santos MA, Sao-Jose C (2008) Phage SPP1 reversible adsorption to *Bacillus subtilis* cell wall teichoic acids accelerates virus recognition of membrane receptor YueB. *J Bacteriol* 190: 4989 – 4996

Brown S, Santa Maria JP Jr, Walker S (2013) Wall teichoic acids of gram-positive bacteria. *Annu Rev Microbiol* 67: 313 – 336

Cao M, Helmann JD (2004) The *Bacillus subtilis* extracytoplasmic-function sigmaX factor regulates modification of the cell envelope and resistance to cationic antimicrobial peptides. *J Bacteriol* 186: 1136 – 1146

Chanishvili N (2012) Phage therapy-history from Twort and d'Herelle through Soviet experience to current approaches. *Adv Virus Res* 83: 3 – 40

Cohen D, Melamed S, Millman A, Shulman G, Oppenheimer-Shaanan Y, Kacen A, Doron S, Amitai G, Sorek R (2019) Cyclic GMP-AMP signalling protects bacteria against viral infection. *Nature* 574: 691 – 695

d'Hérelles F (1917) Sur un microbe invisible antagoniste des bacilles dysentériques. *C R Acad Sci Paris* 165: 373 – 375

Doron S, Melamed S, Ofir G, Leavitt A, Lopatina A, Keren M, Amitai G, Sorek R (2018) Systematic discovery of antiphage defense systems in the microbial pangenome. *Science* 359: eaar4120

Ellis EL, Delbruck M (1939) The growth of bacteriophage. *J Gen Physiol* 22: 365 – 384

Fernandes S, Labarde A, Baptista C, Jakutyte L, Tavares P, Sao-Jose C (2016) A non-invasive method for studying viral DNA delivery to bacteria reveals key requirements for phage SPP1 DNA entry in *Bacillus subtilis* cells. *Virology* 495: 79 – 91

Gallucci S, Matzinger P (2001) Danger signals: SOS to the immune system. *Curr Opin Immunol* 13: 114 – 119

Gao L, Altae-Tran H, Bohning F, Makarova KS, Segel M, Schmid-Burgk JL, Koob J, Wolf YI, Koonin EV, Zhang F (2020) Diverse enzymatic activities mediate antiviral immunity in prokaryotes. *Science* 369: 1077 – 1084

Gottesman S (2019) Trouble is coming: signaling pathways that regulate general stress responses in bacteria. *J Biol Chem* 294: 11685 – 11700

Habusha M, Tzipilevich E, Fiyaksel O, Ben-Yehuda S (2019) A mutant bacteriophage evolved to infect resistant bacteria gained a broader host range. *Mol Microbiol* 111: 1463 – 1475

Hampton HG, Watson BNJ, Fineran PC (2020) The arms race between bacteria and their phage foes. *Nature* 577: 327 – 336

Harwood CR, Cutting SM (1990) *Molecular biological methods for Bacillus*. Chichester, New York: Wiley

Heil M, Land WG (2014) Danger signals – damaged-self recognition across the tree of life. *Front Plant Sci* 5: 578

Helmann JD (2002) The extracytoplasmic function (ECF) sigma factors. *Adv Microb Physiol* 46: 47 – 110

Helmann JD (2016) *Bacillus subtilis* extracytoplasmic function (ECF) sigma factors and defense of the cell envelope. *Curr Opin Microbiol* 30: 122 – 132

Ho TD, Ellermeier CD (2012) Extra cytoplasmic function sigma factor activation. *Curr Opin Microbiol* 15: 182 – 188

Huang X, Decatur A, Sorokin A, Helmann JD (1997) The *Bacillus subtilis* sigma (X) protein is an extracytoplasmic function sigma factor contributing to survival at high temperature. *J Bacteriol* 179: 2915 – 2921

Huang X, Helmann JD (1998) Identification of target promoters for the *Bacillus subtilis* sigma X factor using a consensus-directed search. *J Mol Biol* 279: 165 – 173

Ingmer H, Gerlach D, Wolz C (2019) Temperate phages of *Staphylococcus aureus*. *Microbiol Spectr* 7: GPP3-0058-2018

Isaacs A, Lindenmann J (1957) Virus interference. I. The interferon. *Proc R Soc Lond B Biol Sci* 147: 258 – 267

Jakutyte L, Lurz R, Baptista C, Carballido-Lopez R, Sao-Jose C, Tavares P, Daugelavicius R (2012) First steps of bacteriophage SPP1 entry into *Bacillus subtilis*. *Virology* 422: 425 – 434

Kingston AW, Liao X, Helmann JD (2013) Contributions of the sigma(W), sigma(M) and sigma(X) regulons to the lantibiotic resistome of *Bacillus subtilis*. *Mol Microbiol* 90: 502 – 518

Kovacs M, Halfmann A, Fedtke I, Heintz M, Peschel A, Vollmer W, Hakenbeck R, Bruckner R (2006) A functional *dlt* operon, encoding proteins required for incorporation of D-alanine in teichoic acids in gram-positive bacteria, confers resistance to cationic antimicrobial peptides in *Streptococcus pneumoniae*. *J Bacteriol* 188: 5797 – 5805

Labrie SJ, Samson JE, Moineau S (2010) Bacteriophage resistance mechanisms. *Nat Rev Microbiol* 8: 317 – 327

Levin-Reisman I, Gefen O, Fridman O, Ronin I, Shwa D, Sheftel H, Balaban NQ (2010) Automated imaging with ScanLag reveals previously undetectable bacterial growth phenotypes. *Nat Methods* 7: 737 – 739

Lindberg AA (1973) Bacteriophage receptors. *Annu Rev Microbiol* 27: 205 – 241

Liu J, Gefen O, Ronin I, Bar-Meir M, Balaban NQ (2020) Effect of tolerance on the evolution of antibiotic resistance under drug combinations. *Science* 367: 200 – 204

Ma D, Wang Z, Merrikh CN, Lang KS, Lu P, Li X, Merrikh H, Rao Z, Xu W (2018) Crystal structure of a membrane-bound O-acyltransferase. *Nature* 562: 286 – 290

Makarova KS, Wolf YI, Snir S, Koonin EV (2011) Defense islands in bacterial and archaeal genomes and prediction of novel defense systems. *J Bacteriol* 193: 6039 – 6056

Mamou G, Malli Mohan GB, Rouvinski A, Rosenberg A, Ben-Yehuda S (2016) Early developmental program shapes colony morphology in bacteria. *Cell Rep* 14: 1850 – 1857

McNab F, Mayer-Barber K, Sher A, Wack A, O'Garra A (2015) Type I interferons in infectious disease. *Nat Rev Immunol* 15: 87 – 103

Morehouse BR, Govande AA, Millman A, Keszei AFA, Lowey B, Ofir G, Shao S, Sorek R, Kranzusch PJ (2020) STING cyclic dinucleotide sensing originated in bacteria. *Nature* 586: 429 – 433

Patterson AG, Yevstigneyeva MS, Fineran PC (2017) Regulation of CRISPR-Cas adaptive immune systems. *Curr Opin Microbiol* 37: 1 – 7

Percy MG, Grundling A (2014) Lipoteichoic acid synthesis and function in gram-positive bacteria. *Annu Rev Microbiol* 68: 81 – 100

Perego M, Glaser P, Minutello A, Strauch MA, Leopold K, Fischer W (1995) Incorporation of D-alanine into lipoteichoic acid and wall teichoic acid in *Bacillus subtilis*. Identification of genes and regulation. *J Biol Chem* 270: 15598 – 15606

Saar-Dover R, Bitler A, Nezer R, Shmuel-Galia L, Firon A, Shimoni E, Trieu-Cuot P, Shai Y (2012) D-alanylation of lipoteichoic acids confers resistance to cationic peptides in group B *streptococcus* by increasing the cell wall density. *PLoS Pathog* 8: e1002891

Salas M (2012) My life with bacteriophage phi29. *J Biol Chem* 287: 44568 – 44579

Salmond GP, Fineran PC (2015) A century of the phage: past, present and future. *Nat Rev Microbiol* 13: 777 – 786

Sao-Jose C, Baptista C, Santos MA (2004) *Bacillus subtilis* operon encoding a membrane receptor for bacteriophage SPP1. *J Bacteriol* 186: 8337 – 8346

Schachtele CF, Oman RW, Anderson DL (1970) Effect of elevated temperature on deoxyribonucleic acid synthesis in bacteriophage phi-29-infected *Bacillus amyloliquefaciens*. *J Virol* 6: 430 – 437

Simanski M, Glaser R, Koten B, Meyer-Hoffert U, Wanner S, Weidenmaier C, Peschel A, Harder J (2013) *Staphylococcus aureus* subverts cutaneous defense by D-alanylation of teichoic acids. *Exp Dermatol* 22: 294 – 296

Storz G (2016) New perspectives: Insights into oxidative stress from bacterial studies. *Arch Biochem Biophys* 595: 25 – 27

Sumrall ET, Keller AP, Shen Y, Loessner MJ (2020) Structure and function of *Listeria* teichoic acids and their implications. *Mol Microbiol* 113: 627 – 637

Twort FW (1914) An investigation on the nature of ultra-microscopic viruses. *Lancet* 186: 1241 – 1243

Tzipilevich E, Benfey PN (2021) Phage-Resistant Bacteria Reveal a Role for Potassium in Root Colonization. *MBio* 12: e0140321

Tzipilevich E, Habusha M, Ben-Yehuda S (2017) Acquisition of phage sensitivity by bacteria through exchange of phage receptors. *Cell* 168: 186 – 199.e12

Young FE (1967) Requirement of glucosylated teichoic acid for adsorption of phage in *Bacillus subtilis 168*. *Proc Natl Acad Sci U S A* 58: 2377 – 2384

Young JC, Dill BD, Pan C, Hettich RL, Banfield JF, Shah M, Fremaux C, Horvath P, Barrangou R, Verberkmoes NC (2012) Phage-induced expression of CRISPR-associated proteins is revealed by shotgun proteomics in *Streptococcus thermophilus*. *PLoS One* 7: e38077

Youngman P, Perkins JB, Losick R (1984) A novel method for the rapid cloning in *Escherichia coli* of *Bacillus subtilis* chromosomal DNA adjacent to Tn917 insertions. *Mol Gen Genet* 195: 424 – 433

